Available online at www.sciencedirect.com
SCIENCE DIRECT®
Archives of Biochemistry and Biophysics 424 (2004) 154–162
ABB
www.elsevier.com/locate/yabbi

Phosphotyrosyl peptides and analogues as substrates and inhibitors of purple acid phosphatases

Mohsen Valizadeh,[a] Gerhard Schenk,[b] Kevin Nash,[a] Geoff W. Oddie,[a] Luke W. Guddat,[a] David A. Hume,[c] John de Jersey,[a] Terrence R. Burke Jr.,[d] and Susan Hamilton[a,*]

[a] *Department of Biochemistry, The University of Queensland, St. Lucia, Qld 4072, Australia*
[b] *Department of Chemistry, The University of Queensland, St. Lucia, Qld 4072, Australia*
[c] *Institute for Molecular Biosciences, The University of Queensland, St. Lucia, Qld 4072, Australia*
[d] *Laboratory of Medicinal Chemistry, Division of Basic Sciences, National Institutes of Health, Bethesda, MD 20892, USA*

Received 14 November 2003, and in revised form 23 December 2003

Abstract

Purple acid phosphatases are metal-containing hydrolases. While their precise biological role(s) is unknown, the mammalian enzyme has been linked in a variety of biological circumstances (e.g., osteoporosis) with increased bone resorption. Inhibition of the human enzyme is a possible strategy for the treatment of bone-resorptive diseases such as osteoporosis. Previously, we determined the crystal structure of pig purple acid phosphatase to 1.55 Å and we showed that it is a good model for the human enzyme. Here, a study of the pH dependence of its kinetic parameters showed that the pig enzyme is most efficient at pH values similar to those encountered in the osteoclast resorptive space. Based on the observation that phosphotyrosine-containing peptides are good substrates for pig purple acid phosphatase, peptides containing a range of phosphotyrosine mimetics were synthesized. Kinetic analysis showed that they act as potent inhibitors of mammalian and plant purple acid phosphatases, with the best inhibitors exhibiting low micromolar inhibition constants at pH 3–5. These compounds are thus the most potent organic inhibitors yet reported for the purple acid phosphatases.

Keywords: Purple acid phosphatase; Tartrate resistant acid phosphatase; Inhibition and kinetic studies; Phosphotyrosyl peptide; Osteoporosis

Purple acid phosphatases are a group of nonspecific phosphomonoesterases, members of which have been characterized from animal, plant, and fungal sources (for a recent review see Klabunde and Krebs [1]). An extensive sequence database search has indicated that purple acid phosphatases also occur in a limited number of bacterial organisms (e.g., some cyano- and mycobacteria) [2]. Purple acid phosphatases contain a binuclear Fe^{III}–Me^{II} center in the active site (where Me^{II}=Fe^{II}, Zn^{II} or Mn^{II}) and are distinguished from other acid phosphatases by their characteristic purple color in concentrated solution, due to the presence of a tyrosine → Fe^{III} charge transfer transition. The animal enzymes are also distinguished from lysosomal and prostatic acid phosphatases by their resistance to inhibition by L(+)tartrate and are commonly referred to as "tartrate-resistant acid phosphatases" (TRAPs). Purple acid phosphatase activity, the most commonly used histochemical marker for osteoclasts, is expressed at high levels by these cells [3]. The enzyme is secreted into the resorptive space and there is evidence that it is required for normal bone resorption. Serum levels are elevated in patients with metabolic bone diseases such as osteoporosis and cancers with bone metastases [4]. A transgenic mouse in which the enzyme is overexpressed [5] exhibits increased bone turnover and thus resorption (osteoporosis), while the transgenic mouse knock-out [6] exhibits the opposite phenotype (osteopetrosis). Additionally, in an in vitro bone resorption assay molybdate, an inhibitor of PAP,[1] and a

* Corresponding author. Fax: +11-61-7-3365-4699.
E-mail address: susan.hamilton@mailbox.uq.edu.au (S. Hamilton).

[1] *Abbreviations used:* FOMT, 4′-*O*-(2-fluoromalonyl)-L-tyrosine; F_2Pmp, phosphono(difluoromethyl)phenylalanine; OMT, 4′-*O*-(2-malonyl)-L-tyrosine; PAP, purple acid phosphatase; Pmp, phosphonomethylphenylalanine; PTyr, phosphotyrosine; RKB PAP, red kidney bean purple acid phosphatase; SP PAP, sweet potato purple acid phosphatase.

0003-9861/$ - see front matter © 2004 Published by Elsevier Inc.
doi:10.1016/j.abb.2004.01.008

PAP-specific antibody inhibit bone resorption [7]. It has been speculated that purple acid phosphatase participates in bone resorption either by dephosphorylation of bone matrix proteins such as osteopontin [8] or, since purple acid phosphatase is a redox-active di-iron protein, by producing free oxygen radicals using Fenton chemistry [9].

Despite the fact that purple acid phosphatase is a logical target for drugs suitable for the treatment of bone-resorptive diseases, little attention has been given to the development of specific inhibitors for this enzyme. The synthesis of a series of naphthalenemethylphosphonic acid derivatives has been reported, one of which, bis-benzoyl-1-naphthylmethylphosphonic acid, exhibited an IC_{50} of 1.4 μM. Phosphonates contain a stable phosphorus carbon bond in place of the hydrolyzable carbon oxygen phosphate ester bond. Such compounds, while they may be dead end inhibitors of the enzyme, do not exhibit the desired level of specificity for an effective drug and may also be toxic. We have therefore examined alternative strategies for the development of specific inhibitors of the mammalian purple acid phosphatases, based on our knowledge of the specificity of the enzyme as a phosphotyrosyl protein phosphatase [10]. We have previously shown that phosphotyrosine (PTyr) and the PTyr-containing peptide Fmoc-EEY(P)AA are excellent substrates for mammalian purple acid phosphatases, especially in the low pH range typical of the osteoclastic space (2.5–3) [10,11]. We now report (i) an analysis of the pH dependence of the kinetic parameters for pig purple acid phosphatase, (ii) the results of extended substrate specificity studies on this enzyme using phosphopeptides, and (iii) the development of inhibitors based on one of the best substrates, Fmoc-EY(P)A (Scheme 1A). Four PTyr analogues phosphonomethylphenylalanine (Pmp), phosphono(difluoromethyl)phenylalanine (F_2Pmp), 4′-*O*-(2-malonyl)-L-tyrosine (OMT), and 4′-*O*-(2-fluoromalonyl)-L-tyrosine (FOMT) have been incorporated into the peptide in place of PTyr (Scheme 1B). Additional modifications are the substitution of the C-terminal alanine by leucine, the conversion of the C-terminal carboxy group by an amide, and various substitutions in the PTyr moiety (Scheme 1C). Inhibition by the peptides has been examined using native pig purple acid phosphatase and the recombinant human and mouse enzymes [11], as well as two plant purple acid phosphatases, one from red kidney bean [12] and one from sweet potato [13]. Additionally, the inhibitory effect of some of these peptides was determined for metal ion derivatives of pig purple acid phosphatase. In the absence of crystallographic data for the enzyme–inhibitor complex, computational docking of the inhibitor Fmoc-E(F_2Pmp)A at the active site of the pig enzyme has been undertaken to visualize interactions important for efficient binding of the antagonist.

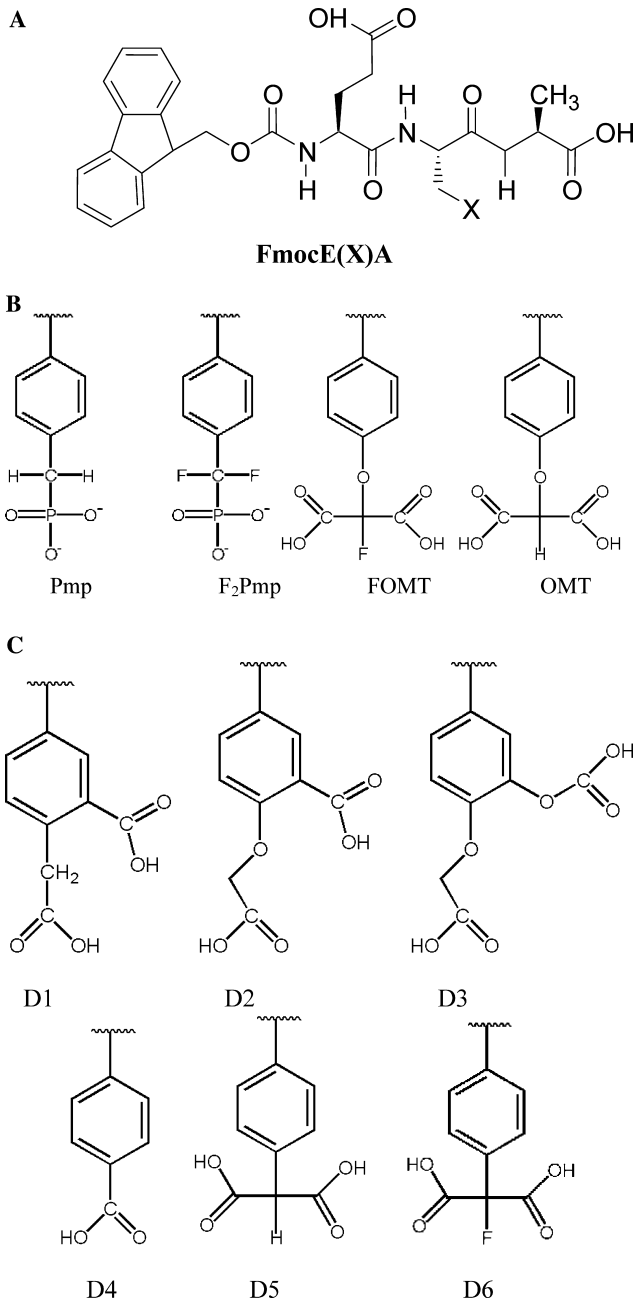

Scheme 1.

Materials and methods

Materials and synthesis of peptides

All chemicals, unless otherwise stated, were of analytical grade. Reagents for peptide synthesis were obtained from Auspep, except for protected PTyr analogues, which were synthesized as described previously: N^{α}-Fmoc-(*O*,*O*-di-*t*-butyl)Pmp [14], N^{α}-Fmoc-(*O*,*O*-diethyl) F_2Pmp [15], N^{α}-Fmoc-OMT-*O*,*O*-(*tert*-butyl)$_2$ [16], and N^{α}-Fmoc-FOMT-*O*,*O*-(*tert*-butyl)$_2$ [17]. PTyr-containing peptides were synthesized as described

previously [10]. PTyr mimetics were incorporated into peptides of the general formula Fmoc-EXA, where X represents the PTyr mimetic, using manual solid phase peptide synthesis as described previously [10]. An exception was the synthesis of the F_2Pmp compound where deprotection was carried out as described by Otaka et al. [18]. Peptides were purified by reverse phase HPLC and mass spectra were recorded as described previously [10].

Protein purification and enzyme kinetics

Purple acid phosphatases from pig allantoic fluid [19], red kidney bean [12], and sweet potato [13] and recombinant human and mouse from baculovirus-infected insect cells [11] were prepared as described previously. All enzyme preparations were at least 95% pure, as judged by SDS–PAGE analysis and specific activity. The mammalian enzymes were reduced to their fully active forms by incubation of stock solutions (~2 mg/ml) in 0.1 M acetate buffer, pH 4.90, with 58 mM ferrous ammonium sulfate and 140 mM β-mercaptoethanol [20]. Excess reducing agent was diluted ~1000-fold upon addition of the enzyme to the steady state rate assays. Metal ion replacements for pig purple acid phosphatase were carried out according to the method of Beck et al. [20]. Kinetics of hydrolysis of phosphopeptides and determination of the molar concentration of pig purple acid phosphatase used for the calculation of k_{cat} were performed as described previously [10]. The pH dependence of the kinetic parameters for Fe^{III}–Fe^{II} pig purple acid phosphatase was determined in 0.1 M glycine buffer (pH 2.0–3.5), 0.1 M acetate buffer (pH 3.5–6.0), and 0.1 M Mes buffer (pH 6.0–7.0), using varying concentrations of *p*-NPP or L-PTyr. The kinetic data were analyzed using the rapid equilibrium diprotic model [21]. Kinetics of inhibition at pH 3.30 and 4.90 were analyzed using L-PTyr as substrate [10]. For each inhibitor, initial rates, monitored at 280 nm, were determined using a minimum of three inhibitor concentrations in the range 1–100 μM depending on the K_i, and for each inhibitor concentration at a range of substrate concentrations (0.1–10 mM) depending on the apparent K_m. Kinetic constants were obtained by nonlinear fit to the Michaelis–Menten equation with competitive inhibition, using DNRPEASY [22].

Modelling strategy

Protons were added to the 1.55 Å resolution crystal structure of the pig enzyme (1UTE in the protein data bank [23]) using BIOPOLYMER, a module of INSIGHT 2000.1 (Accelrys). For this process, it was assumed that the protein was at pH 3.5. Three-dimensional models of the inhibitors were constructed using SKETCHER in INSIGHT 2000.1 and then were energy minimized. The docking of the inhibitors to the protein was performed using GOLD and followed the standard protocol as described by Jones et al. [24].

Results and discussion

Dependence of kinetics parameters of Fe^{III}–Fe^{II} pig purple acid phosphatase on pH

The pH dependence of the enzyme-catalyzed hydrolysis of pNPP and L-PTyr is shown in Fig. 1. The kinetic parameters and approximate pK_a values obtained by fitting the data using the diprotic model are summarized in Table 1. Consistent with previous reports for the pig and red kidney bean enzymes [25], k_{cat} exhibits a maximum at pH ~5.0 for both substrates (Figs. 1A and C). In contrast, catalytic efficiency (k_{cat}/K_m) reaches its optimum in the range between pH 3 and 3.5, the pH range typically found in the osteoclastic resorptive space. The lower pH optimum for k_{cat}/K_m results from the decrease in K_m across the entire pH range under investigation. It should be emphasized, however, that the pK_a values in Table 1 are approximate, especially in the low pH range where data are limited.

Interpretation of the pH dependencies is complex because of the ionizable nature of the substrate and because the pK_a values are not sufficiently well separated to allow precise determination. However, some tentative conclusions may be drawn. The protonation equilibria pK_{es1} and pK_{es2} correspond to residues in the enzyme–substrate complex, which control catalysis [21]. The pK_a of ~4 (pK_{es1}) may correspond to the ionization of a water molecule bound to Fe^{III}. The pK_a of water coordinated to ferric ion in model complexes is ~3 [26]. The assignment is consistent with spectroscopic studies of the interaction of phosphates with the bovine and pig enzymes [25,27–30], which revealed an ionization occurring in the pH range 3.9–4.8. The conjugate base, a coordinated hydroxyl group, is a potential candidate for the attacking nucleophile in hydrolysis [25,29–31]. The pK_{es2} value of ~6 may correspond to a residue in the active site acting as a general acid to protonate the leaving group on hydrolysis. Residues previously identified as candidates, based on the crystal structures of the pig and red kidney bean enzymes, are the conserved His92 and His195 (pig enzyme numbering), which are within hydrogen bonding distance of bound phosphate [23,32].

The equilibrium constants pK_{e1} and pK_{e2} correspond to residues in the free enzyme or the substrate, which control substrate binding and/or catalysis [21]. The low pK_{e1} of ~2 may reflect the deprotonation of a water molecule bridging the metal ions in the active site. The presence of a bridging μ-hydroxo group in the active purple acid phosphatases from pig, bovine, and red kidney bean is supported by saturation magnetization

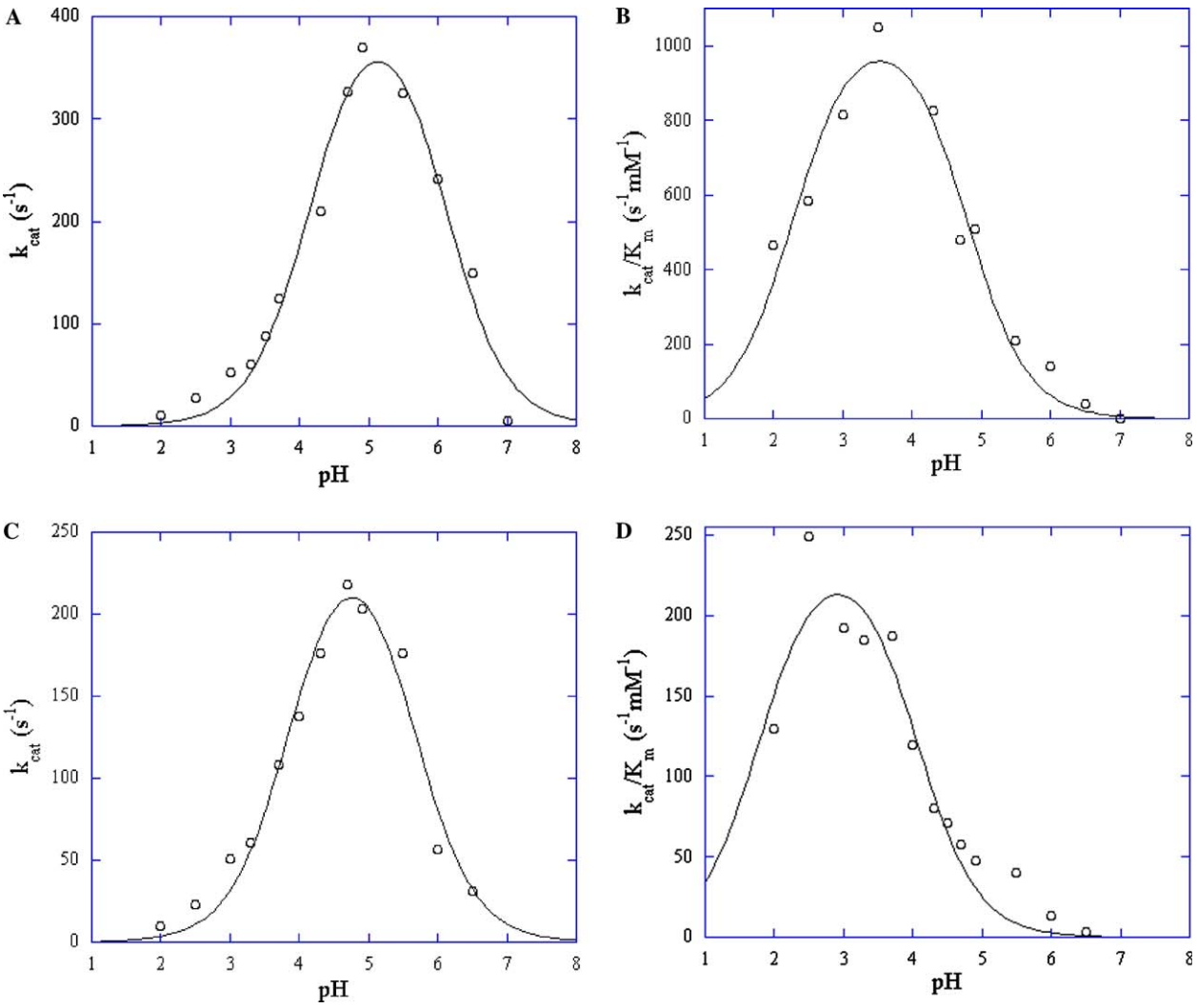

Fig. 1. Kinetic parameters (k_{cat} and k_{cat}/K_m) as a function of pH for Fe^{III}–Fe^{II} pig purple acid phosphatase using pNPP (A and B, respectively) and PTyr (C and D, respectively) as substrates. The data were quantitatively analyzed using equations derived from the diprotic model [21].

Table 1
Kinetic parameters[a] determined for Fe^{III}–Fe^{II} pig purple acid phosphatase using pNPP and PTyr as substrates

Substrate	k_{cat} (s^{-1})	K_s (mM)	pK_{e1}	pK_{e2}	pK_{es1}	pK_{es2}
pNPP	431	1.23	2.28	4.77	4.15	6.11
PTyr	256	1.03	1.83	4.09	3.85	5.68

[a] Kinetic data (k_{cat}, K_m, and k_{cat}/K_m) measured at pH values ranging from 2 to 7 were analyzed using the diprotic model [21], resulting in estimates for the protonation equilibria for free enzyme (pK_{e1} and pK_{e2}) and the enzyme–substrate complex (pK_{es1} and pK_{es2}). K_S, the constant describing the equilibrium between free enzyme and the ES complex, is assumed to be independent of the protonation state of the enzyme.

measurements, which indicated weak exchange coupling [33,34]. A role as the attacking nucleophile has been attributed to this bridging group as an alternative to the hydroxo group coordinated to ferric ion [35–38]. The pK_a of ~2 could alternatively be due to the first ionization of the substrate, although we would expect the value to be lower—the first acid dissociation of phenyl phosphate is reported to be 0.3 [25].

Hydrolysis of phosphopeptide substrates

Kinetic data for the hydrolysis of a range of phosphopeptides by pig purple acid phosphatase are given in Table 2. As noted previously [10], inclusion of the Fmoc group at the N-terminus led to a significant decrease in K_m at pH 2.5 and 4.9, suggesting the presence of a hydrophobic pocket in the vicinity of the active site.

Table 2
Hydrolysis of phosphopeptides by pig purple acid phosphatase[a]

Substrate	k_{cat} (s^{-1}), K_m (μM)	
	pH 2.50	pH 4.90
EEY(P)AA	65 ± 5, 140 ± 10	79 ± 1, 310 ± 10
Fmoc-EEY(P)AA	35 ± 2, 6 ± 1	120 ± 5, 75 ± 5
Fmoc-EY(P)A	25 ± 0.5, 8 ± 0.5	31 ± 0.5, 48 ± 2
Fmoc-AAY(P)AA	ND	100 ± 20, 120 ± 20
Fmoc-KKY(P)AA	ND	170 ± 40, 950 ± 200

[a] Measured at 25 °C in 0.1 M acetate buffer, pH 4.90, or 0.1 M glycine buffer, pH 2.50. ND, not determined.

Table 4
Inhibition of pig PAP by selected peptides

Inhibitor	pH 3.3		pH 4.9	
	[a]$K_{i(c)}$ (μM)	$K_{i(uc)}$ (μM)	$K_{i(c)}$ (μM)	$K_{i(uc)}$ (μM)
FmocE(OMT)A	6 ± 1	—	38 ± 1	—
FmocE(OMT) A-amide	24 ± 3	—	182 ± 16	—
FmocE(OMT)L	8 ± 1	190 ± 9	49 ± 4	—
FmocE(OMT) L-amide	5 ± 1	—	18 ± 1	—

[a] $K_{i(c)}$ and $K_{i(uc)}$ are the competitive and uncompetitive inhibition constants, respectively.

Replacement of the Glu residues in the substrate with Ala caused only negligible change in K_m, whereas replacement by Lys led to an increase in K_m of ~12-fold at pH 4.90. For all peptides, K_m values were lower and k_{cat}/K_m values were higher at pH 2.50 than 4.90, consistent with the pH dependencies seen for pNPP and PTyr (Table 1). The lowest K_m values for the peptides Fmoc-EY(P)A and Fmoc-EEY(P)AA were in the low micromolar range at pH 2.5, suggesting that the peptides provided a good starting point for the synthesis of substrate analogues containing PTyr mimetics. Since Fmoc-EY(P)A was almost as good a substrate as Fmoc-EEY(P)AA and exhibited the same K_m within experimental error, it was used as the parent compound for the synthesis of the inhibitors.

Inhibition of purple acid phosphatases

The substrate analogues based on Fmoc-EY(P)A (Scheme 1) are all potent inhibitors of Fe–Fe pig purple acid phosphatase. The K_i values (summarized in Table 3) are lower at pH 3.30 than 4.90 and are in the micromolar range, comparable with the K_m values for the substrate on which these inhibitors are based (Table 2). These peptides are thus very effective inhibitors of the enzymes, comparable at least with the best of the naphthalenemethylphosphonic acid derivatives [39]. The inhibitory effect of these analogues was also assessed for the recombinant human and mouse purple acid phosphatases [11], as well as the enzymes isolated from red kidney bean [12] and sweet potato [13]. The K_i values are in the range from 1 to 100 μM. These inhibitors are in general more potent at low pH, a desirable property for their further use in the development of drugs against bone-resorptive disorders (pH in osteoclastic space ranges from 2.5 to 3). Fluorination of the OMT moiety in the peptide analogue (Scheme 1) leads to a decrease in the inhibitory effect in all but the sweet potato enzyme. The effect of the fluorination of the Pmp moiety displays no clear trend in the inhibition of the mammalian enzymes, however, both plant purple acid phosphatases are inhibited more strongly by the fluorinated analogue, again suggesting stabilizing interactions via H-bonding and/or by positively charged residues.

Increasing the hydrophobicity of the tripeptide had no significant effect on the inhibition of pig purple acid phosphatase. Starting from Fmoc-E(OMT)A the alanine was replaced by leucine. Virtually no differences in inhibition were apparent (Table 4). For the Fmoc-E(OMT)A/L series replacing the C-terminal carboxylate by an amide group affected the potency of the inhibitors only mildly. The largest effect on inhibition was achieved by modifying the tyrosine moiety (Scheme 1C and Table 5). Substitution at the C5 position of the aromatic ring with carboxy- and acetoxy groups greatly reduces the binding affinity of the OMT-containing inhibitor (D1–D3), probably due to steric interactions. However, replacing the *O*-malonyl group by formyl (D4), and thus preventing the interaction of this OMT inhibitor with

Table 3
Inhibition of PAPs by phosphotyrosyl analogs ([a]$K_{i(c)}$ and $K_{i(uc)}$ values in μM)

Enzyme	FmocEY(Pmp)A				FmocEY(F_2Pmp)A				FmocE(OMT)A				FmocE(FOMT)A			
	pH 3.3		pH 4.9		pH 3.3		pH 4.9		pH 3.3		pH 4.9		pH 3.3		pH 4.9	
	$K_{i(c)}$	$K_{i(uc)}$	$K_{i(c)}$	$K_{i(uc)}$	$K_{i(c)}$	$K_{i(uc)}$	$K_{i(c)}$	$K_{i(uc)}$	$K_{i(c)}$	$K_{i(uc)}$	$K_{i(c)}$	$K_{i(uc)}$	$K_{i(c)}$	$K_{i(uc)}$	$K_{i(c)}$	$K_{i(uc)}$
Human PAP	ND	ND	ND	ND	67	—	63	—	14	—	26	—	36	23	74	—
Mouse PAP	8	13	50	143	18	—	62	—	2.9	—	62	—	55	70	15	—
Pig PAP	53	—	85	—	14	—	87	—	1.9	—	47	—	12	38	50	—
RKB PAP	77	—	66	—	7	—	29	—	0.9	6.8	41	—	31	—	15	—
SP PAP	83	—	105	—	23	—	80	—	5.8	—	81	—	0.9	—	17	—

ND not determined.
[a] $K_{i(c)}$ and $K_{i(uc)}$ are the competitive and uncompetitive inhibition constants, respectively.

Table 5
Inhibition of pig PAP by derivatives of FmocE(OMT)L-amide

Inhibitor	pH 3.3		pH 4.9	
	[b]$K_{i(c)}$ (μM)	$K_{i(uc)}$ (μM)	$K_{i(c)}$ (μM)	$K_{i(uc)}$ (μM)
FmocE(OMT) L-amide	5 ± 1	—	18 ± 1	—
FmocE(D1)L-amide[a]	201 ± 12	—	279 ± 3	—
FmocE(D2)L-amide[a]	112 ± 11	—	146 ± 14	—
FmocE(D3)L-amide[a]	413 ± 18	—	777 ± 37	—
FmocE(D4)L-amide[a]	100 ± 1	—	161 ± 2	—
FmocE(D5)L-amide[a]	6 ± 1	—	38 ± 1	—
FmocE(D6)L-amide[a]	8 ± 1	190 ± 11	49 ± 4	—

[a] D1 to D6 refer to the aromatic side chains shown in Scheme 1C.
[b] $K_{i(c)}$ and $K_{i(uc)}$ are the competitive and uncompetitive inhibition constants, respectively.

both metal ions, also strongly deteriorates its inhibitory effect (Table 5). This suggests that bidentate binding of the substrate analogue is crucial to achieve specific and strong inhibition. Consistently, the replacement of the *O*-malonyl group by malonyl (D5 and D6) displays only a minor effect, since the slightly shorter side chain may still be able to bind to both metal ions simultaneously. Again fluorination leads to an increase in K_i (D6).

The effect of changing the metal centers on inhibition has also been examined. Fe^{III}–Zn^{II} and Fe^{III}–Mn^{II} derivatives of pig purple acid phosphatase (which mimic the binuclear centers in red kidney bean and sweet potato purple acid phosphatases, respectively [40,41]) were generated according to published procedures [20,30], and inhibition data were collected for both the OMT- and the FOMT-containing tripeptides (Scheme 1) at pH 3.3 and 4.9. The results are summarized in Table 6. Replacing Fe^{II} by Zn^{II} does increase the affinity of pig purple acid phosphatase for these inhibitors, approaching the K_i values obtained for the red kidney bean enzyme (Table 3). The affinity of the Fe^{III}–Mn^{II} derivative of pig purple acid phosphatase for OMT is moderately weaker than that of the native pig enzyme, resembling that of sweet potato purple acid phosphatase. However, for FOMT both an increase in its inhibitory potency and the type of inhibition was observed (uncompetitive and noncompetitive at pH 3.3 and 4.9, respectively). A similar trend has been seen for the sweet potato enzyme (Table 3), although the type of inhibition remains competitive. Incorporation of Mn^{II} into the active site of pig purple acid phosphatase may cause some conformational change that affects the binding mode of the fluorinated inhibitor. Attempts to crystallize pig purple acid phosphatase in the presence of OMT and FOMT have not been successful, however, an analysis by molecular modeling of the structure of the native pig enzyme reveals factors which may be important for the determination of inhibition specificity (vide infra).

Inhibitor–protein interactions

We have determined the crystal structure of pig purple acid phosphatase [23] and other groups have solved the structures of the rat enzyme [42,43]. The overall structural features of these mammalian enzymes are very similar, as expected based on the very high degree of sequence identity (>85%) [1]. Furthermore, despite low sequence homology the structure of red kidney bean purple acid phosphatase [32] displays an active site geometry very similar to those of the mammalian enzymes. The seven metal-coordinating amino acids are invariant and binding of the substrate leads to the formation of a μ-phosphate complex. However, apart from the binding of the phosphate group the interactions between substrate and protein are still poorly understood. The following features in the active site of pig purple acid phosphatase may play an important role in the interactions between protein and substrate/inhibitor. The two Fe atoms lie at the base of a cavity (Fig. 2) approximately 7 Å deep. The length of the cavity, which extends from the NE2 atom of Glu151 to the CZ atom of Phe 244, is 11.4 Å. The maximum width of the cavity (from the CE1 atom of His195 to the OD1 atom of Asp146) is 7 Å. The side chains of the metal binding ligands His221, His223, Tyr55, and Asn91 form a shelf that protrudes outward from the Fe atom base. The four metal binding atoms of these ligands form the corners of a rectangle 6.4 Å by 3.2 Å. The outer layer of the active site consists of eight residues, which have their

Table 6
Inhibition of metal ion derivatives of pig PAP by OMT- and FOMT-containing peptides

Metal content	Inhibitor	pH 3.3		pH 4.9	
		[a]$K_{i(c)}$ (μM)	$K_{i(uc)}$ (μM)	$K_{i(c)}$ (μM)	$K_{i(uc)}$ (μM)
Fe^{III}–Fe^{II}	FmocE(OMT)A	6 ± 0.2	—	38 ± 1	—
Fe^{III}–Zn^{II}	FmocE(OMT)A	2.4 ± 0.2	—	1.6 ± 0.2	—
Fe^{III}–Mn^{II}	FmocE(OMT)A	10 ± 1.6	250 ± 20	77 ± 3	—
Fe^{III}–Fe^{II}	FmocE(FOMT)A	12 ± 1.6	38 ± 4	50 ± 2	—
Fe^{III}–Zn^{II}	FmocE(FOMT)A	0.8 ± 0.1	—	16 ± 0.6	—
Fe^{III}–Mn^{II}	FmocE(FOMT)A	—	1.6 ± 0.2	1.5 ± 0.2	1.2 ± 0.1

[a] $K_{i(c)}$ and $K_{i(uc)}$ are the competitive and uncompetitive inhibition constants, respectively.

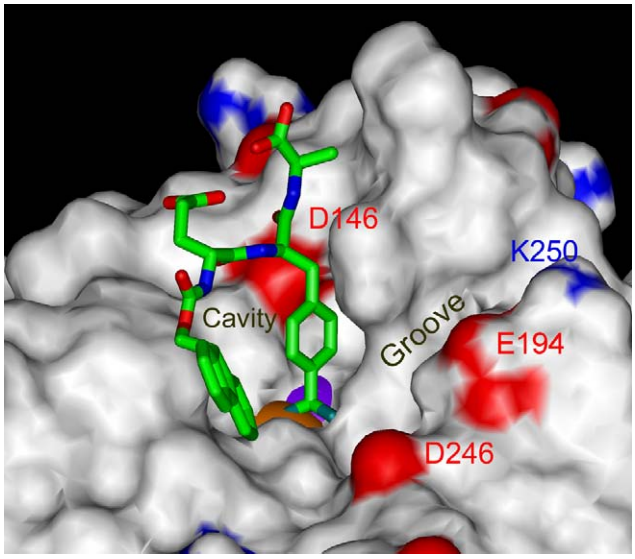

Fig. 2. Proposed interaction of pig purple acid phosphatase and peptide inhibitor. A Connolly surface representation of the active site region. The negatively charged amino acid residues (Asp and Glu) are colored red and the positively charged residues (Lys and Arg) are colored blue. All remaining amino acid residues are colored white. The metal ions are colored tan for Fe^{III} and red for the redox-active $Fe^{II/III}$ and they can be seen just protruding above the surface. The highest ranked docking solution of the F_2PMP peptide to the enzyme is depicted as a stick model and color-coded such that green is for carbon, red for oxygen, blue for nitrogen, and aquamarine for fluorine. The groove on the surface is lined with charged amino acids and may be a region for the development of second generation inhibitors.

side chains directed toward the binuclear metal center. They include residues His92, Phe56, Phe244, Asp246, Glu194, His195, Gln151, and Asp146. The latter residue is part of an exposed loop, only present in mammalian purple acid phosphatases. Proteolytic cleavage within this loop has been associated with a significant increase in enzyme activity for rat and human purple acid phosphatases [37]. Based on site-directed mutagenesis studies, it has been proposed that the H-bond interaction between Asp146 and the Fe^{II} ligand Asn91 is crucial for the regulation of enzyme reactivity [37]; disrupting this interaction completely leads to the strongest catalytic enhancement. This may also be a reason for the variation of inhibition by fluorinated Pmp inhibitors observed for pig and mouse purple acid phosphatases (Table 3). A narrow groove, approximately 5 Å deep (Fig. 2), is connected to the main cavity. It is bordered by Gln151, Ser150, and Gln152 on one side and on the other by Glu194, Lys250, and His 251. Distances across the groove are 5.6 Å between the NE2 atom of His251 and the NE2 atom of Gln152, 7.0 Å between the carbonyl oxygen of Ser150 and the NZ atom of Lys250, and 6.8 Å between the NE2 atom of Gln151 and the OE2 atom of Gln194.

No crystals of enzyme–peptide-inhibitor complexes have yet been obtained. We have therefore docked the inhibitor Fmoc-E(F_2Pmp)A into the active site of the crystal structure of pig purple acid phosphatase. Fig. 2 shows two views of the highest ranked solution found with GOLD. The oxygen atoms from the phosphonate are bound to the iron atoms and complete the octahedral geometry. The aromatic ring of the phosphotyrosyl side chain fits into the cavity (Fig. 2) and makes van der Waals contacts with His195, Asn91, Glu151, and Ser145. In this docking solution, the carboxyl group of the glutamic acid in the F_2Pmp inhibitor forms a hydrogen bond with the two peptide amide groups of the inhibitor. This raises the possibility that the requirement for glutamic acid at this position may be important for peptide conformation, rather than binding to the enzyme. This suggestion is consistent with the observed reduction in binding affinity when this glutamate is replaced by alanine or lysine (Table 2). The glutamic acid in the inhibitor imposes a conformation, where the Fmoc group is able to stack against a hydrophobic patch on the wall of the cavity, which includes Tyr55, Phe56, and Phe244. While the different solutions found using the, GOLD program [24] display considerable variations in spatial orientations (data not shown), the positions of the phosphonotyrosyl side chains are in close agreement, indicating that this part of the substrate analogue undergoes specific interactions with the protein that support tight binding. Modifications within this phosphotyrosine moiety lead to a great increase in the inhibition constant (Table 5). In contrast, for the remainder of the peptide several conformations are possible, suggesting less specific interactions between inhibitor and protein. There are several hydrophobic surfaces where the Fmoc group could potentially be located. Parallel studies with the Fmoc-E(OMT)A peptide docked onto the pig enzyme show a distribution of docking solutions similar to that found for the Fmoc-E(F_2Pmp)A peptide (data not shown). In the top 10 solutions, the OMT group is located in approximately the same orientation as the F_2Pmp moiety and again there are several alternative locations for the Fmoc group. Overall there is good evidence to suggest that the GOLD program has correctly oriented both the OMT and the F_2Pmp groups, whereas the positioning of the Fmoc group remains speculative. In the X-ray structure of pig purple acid phosphatase, this groove is filled by eight ordered water molecules [23], making it a target region that could be exploited for improving inhibitor affinity.

Crystals of human purple acid phosphatase have been produced, but no structural data have been published [44]. However, human and pig enzymes are 88% identical with only seven nonconserved differences. A homology model shows few changes near the active site so that the pig enzyme appears to be a good model for the intact human purple acid phosphatase [23]. Furthermore, as mentioned above, a comparison between the

structures of pig [23], red kidney bean [32], and sweet potato [45] purple acid phosphatases shows that despite overall low sequence homology, the core structures are very similar. Apart from variations in metal ion composition (Fe^{III}–Fe^{II}, Fe^{III}–Zn^{II}, and Fe^{III}–Mn^{II}, respectively), there are variable loops in the vicinity of the active sites, which may contribute to differences in substrate and inhibitor specificity [23,46]. The inhibition data presented here show that various plant and mammalian purple acid phosphatases bind the tripeptide inhibitors with affinities similar to the pig enzyme (Table 4). Both plant and mammalian purple acid phosphatases also have pH-dependent K_i values for all tested inhibitors, with higher binding affinity at lower pH. It is interesting to note that at pH 3.3 the FOMT peptide is a less effective inhibitor than the OMT peptide for most purple acid phosphatases (Table 3). The exception is the Fe- and Mn-containing sweet potato purple acid phosphatase, which has a 4- to 5-fold higher affinity for the FOMT peptide. This inverted behavior may be due, at least in part, to the different metal ion compositions; the Fe^{III}–Mn^{II} derivative of pig purple acid phosphatase also appears to be stronger inhibited by FOMT (Table 6). Furthermore, previous work on the inhibition of PTyr protein phosphatase 1B showed that an FOMT-containing peptide exhibited a 10-fold higher affinity for the enzyme than the corresponding OMT peptide [17], which was attributed in part to an additional hydrogen bond between the fluorine and a group on the enzyme. The pK_a value for the second ionization of the OMT malonyl group is affected by fluorine substitution: ~3.9 for malonyl vs 2.84 for the fluoro derivative [17]. The FOMT peptide would therefore carry a larger negative charge than the OMT peptide, especially at pH 3.3. Finally, phosphate has been shown to bind to the binuclear center of the purple acid phosphatases by bridging the metal ions [23,42,45]. Thus, if the malonyl group bound similarly it might be anticipated that the dianion would bind more effectively than the monoanion. That this is indeed the case is supported by the observation that removal of the malonyl group greatly reduces the binding affinity of the resulting substrate analogues (Table 5).

In conclusion, we have identified high-affinity, peptide-based inhibitors of purple acid phosphatases. While the tripeptide and Fmoc parts of the inhibitors contribute to their overall affinity through moderately specific, hydrophobic interactions, the modified phosphotyrosyl moiety is responsible for both tight and specific binding to the active site. The presented substrate analogues are potent inhibitors for all purple acid phosphatases and may prove valuable [1] in the development of chemotherapeutic agents against osteoporosis and [2] in probing the specificity of purple acid phosphatase as a phosphotyrosyl protein phosphatase. Since the physiological substrate(s) and function(s) of purple acid phosphatases are unknown, this may provide insight into the role of these enzymes. Of particular interest is the observation that these tripeptide-based inhibitors are most potent at pH values similar to those measured in the osteoclastic space (~3). Further improvement of the potency of this group of inhibitors may be achieved once crystallographic data of purple acid phosphatases with bound analogues become available.

Acknowledgments

This work was supported by a Grant-in-Aid from Johnson and Johnson Research Pty Ltd., by the National Health and Medical Research Council and by the Australian Research Council.

References

[1] T. Klabunde, B. Krebs, Struct. Bonding 89 (1997) 177–198.
[2] G. Schenk, M.L.J. Korsinczky, D.A. Hume, S. Hamilton, J. de Jersey, Gene 255 (2000) 419–424.
[3] G.W. Oddie, G. Schenk, N.Z. Angel, N. Walsh, L.W. Guddat, J. de Jersey, A.I. Cassady, S.E. Hamilton, D.A. Hume, Bone 27 (2000) 575–584.
[4] D.W. Moss, F.D. Raymond, D.B. Wile, Crit. Rev. Clin. Lab. Sci. 32 (1995) 431–467.
[5] N.Z. Angel, N. Walsh, M.R. Forwood, M.C. Ostrowski, A.I. Cassady, D.A. Hume, J. Bone Miner. Res. 15 (2000) 103–110.
[6] A.R. Hayman, S.J. Jones, A. Boyde, D. Foster, W.H. Colledge, M.B. Carlton, M.J. Evans, T.M. Cox, Development 122 (1996) 3151–3162.
[7] M. Zaidi, B. Moonga, D.W. Moss, I. MacIntyre, Biochem. Biophys. Res. Commun. 159 (1989) 68–71.
[8] B. Ek-Rylander, M. Flores, M. Wendel, D. Heinegård, G. Andersson, J. Biol. Chem. 269 (1994) 14853–14856.
[9] J. Sibille, K. Doi, P. Aisen, J. Biol. Chem. 262 (1987) 59–62.
[10] K. Nash, M. Feldmuller, J. de Jersey, P. Alewood, S. Hamilton, Anal. Biochem. 213 (1993) 303–309.
[11] K. Marshall, K. Nash, G. Haussman, I. Cassady, D. Hume, J. de Jersey, S. Hamilton, Arch. Biochem. Biophys. 345 (1997) 230–236.
[12] J.L. Beck, L.A. McConaghie, A.C. Summors, W.N. Arnold, J. de Jersey, B. Zerner, Biochim. Biophys. Acta 869 (1986) 61–68.
[13] G. Schenk, Y. Ge, L.E. Carrington, C.J. Wynne, I.R. Searle, B.J. Carroll, S. Hamilton, J. de Jersey, Arch. Biochem. Biophys. 370 (1999) 183–189.
[14] T.R. Burke Jr., P. Russ, B. Lim, Synthesis 11 (1991) 1019–1020.
[15] T.R. Burke Jr., M.S. Smyth, A. Ataka, P.P. Roller, Tetrahedron Lett. 34 (1993) 4125–4128.
[16] B. Ye, T.R. Burke Jr., Tetrahedron Lett. 36 (1995) 4733–4736.
[17] T.R. Burke Jr., B. Ye, M. Akamatsu, H.J. Ford, X. Yan, H.K. Kole, G. Wolf, S.E. Shoelson, P.P. Roller, J. Med. Chem. 39 (1996) 1021–1027.
[18] A. Otaka, T.R. Burke Jr., M.S. Smyth, M. Nomizu, P.P. Roller, Tetrahedron Lett. 34 (1993) 7039–7042.
[19] H.D. Campbell, D.A. Dionysius, D.T. Keough, B.E. Wilson, J. de Jersey, B. Zerner, Biochem. Biophys. Res. Commun. 82 (1978) 615–620.
[20] J.L. Beck, D.T. Keough, J. de Jersey, B. Zerner, Biochim. Biophys. Acta 791 (1984) 357–363.

[21] I.H. Segel, Enzyme Kinetics: Behavior and Analysis of Rapid Equilibrium and Steady-State Enzyme Systems, Wiley, New York, 1993.
[22] R.G. Duggleby, Comput. Biol. Med. 14 (1984) 447–455.
[23] L.W. Guddat, A.S. McAlpine, D.A. Hume, S. Hamilton, J. de Jersey, J.L. Martin, Structure 7 (1999) 757–767.
[24] G. Jones, P. Willett, R.C. Glen, A.R. Leach, R. Taylor, J. Mol. Biol. 267 (1997) 727–748.
[25] M. Aquino, J.-S. Lim, A.G. Sykes, J. Chem. Soc. Dalton Trans. (1994) 429–436.
[26] C.F. Baes, E. Mesmer, The Hydrolysis of Cations, Wiley-Interscience, New York, 1976.
[27] B.A. Averill, J.C. Davis, S. Burman, T. Zirino, J. Sanders-Loehr, T.M. Loehr, T. Sage, P.G. Debrunner, J. Am. Chem. Soc. 109 (1987) 3760–3767.
[28] M. Dietrich, D. Münstermann, H. Suerbaum, H. Witzel, Eur. J. Biochem. 199 (1991) 105–113.
[29] M.B. Twitchett, A.G. Sykes, Eur. J. Inorg. Chem. (1999) 2105–2115.
[30] M.B. Twitchett, G. Schenk, M.A.S. Aquino, D.T.-Y. Yiu, T.-C. Lau, A.G. Sykes, Inorg. Chem. 41 (2002) 5787–5794.
[31] X.D. Wang, C.R. Randall, A.E. True, L. Que Jr., Biochemistry 35 (1996) 13946–13954.
[32] T. Klabunde, N. Sträter, R. Fröhlich, H. Witzel, B. Krebs, J. Mol. Biol. 259 (1996) 737–748.
[33] E.P. Day, S.S. David, J. Peterson, W.R. Dunham, J.J. Bonvoisin, R.H. Sands, L. Que Jr., J. Biol. Chem. 263 (1988) 15561–15567.
[34] S. Gehring, P. Fleischhauer, M. Behlendorf, M. Hübner, J. Lorösch, W. Haase, M. Dietrich, R. Löcke, B. Krebs, H. Witzel, Inorg. Chim. Acta 252 (1996) 13–17.
[35] M. Merkx, M.W.H. Pinkse, B.A. Averill, Biochemistry 38 (1999) 9914–9923.
[36] X. Wang, R.Y.N. Ho, A.K. Whiting, L. Que Jr., J. Am. Chem. Soc. 121 (1999) 9235–9236.
[37] E.G. Funhoff, J. Ljusberg, Y. Wang, G. Andersson, B.A. Averill, Biochemistry 40 (2001) 11614–11622.
[38] S.K. Smoukov, L. Quaroni, X. Wang, P.E. Doan, B.M. Hoffman, L. Que Jr., J. Am. Chem. Soc. 124 (2002) 2595–2603.
[39] C.F. Schwender, S.A. Beers, E. Malloy, K. Demarest, L. Minor, K. Lau, Bioorg. Med. Chem. Lett. 5 (1995) 1801–1806.
[40] J.L. Beck, M.J. McArthur, J. de Jersey, B. Zerner, Inorg. Chim. Acta 153 (1988) 39–44.
[41] G. Schenk, C.L. Boutchard, L.E. Carrington, C.J. Noble, B. Moubaraki, K.S. Murray, J. de Jersey, G.R. Hanson, S. Hamilton, J. Biol. Chem. 276 (2001) 19084–19088.
[42] Y. Lindqvist, E. Johansson, H. Kaija, P. Vikho, G. Schneider, J. Mol. Biol. 291 (1999) 135–147.
[43] J. Uppenberg, F. Lindqvist, C. Svensson, B. Ek-Rylander, G. Andersson, J. Mol. Biol. 290 (1999) 201–211.
[44] A.R. Hayman, T.M. Cox, J. Biol. Chem. 269 (1994) 1294–1300.
[45] G. Schenk, L.E. Carrington, S.E. Hamilton, J. de Jersey, L.W. Guddat, Acta Crystallogr. D 55 (1999) 2051–2052.
[46] G. Schenk, L.W. Guddat, L.E. Carrington, D.A. Hume, S. Hamilton, J. de Jersey, Gene 250 (2000) 117–125.